JOURNAL OF COMPUTATIONAL PHYSICS 107, 297–308 (1993)

Central Difference TVD Schemes for Time Dependent and Steady State Problems

P. JORGENSON

NASA Lewis Research Center, Cleveland, Ohio 44135

AND

E. TURKEL

Sackler Faculty of Exact Sciences, Tel-Aviv University, Tel-Aviv 69978, Israel and ICOMP, NASA Lewis Research Center

Received March 10, 1992; revised September 21, 1992

We use central differences to solve the time dependent Euler equations. The schemes are all advanced using a Runge–Kutta formula in time. Near shocks a second difference is added as an artificial viscosity. This reduces the scheme to a first-order upwind scheme at shocks. The switch that is used guarantees that the scheme is TVD. For steady state problems it is usually advantageous to relax this condition. Then small oscillations do not activate the switches and the convergence to a steady state is improved. To sharpen the shocks different coefficients are needed for different equations, so a matrix-valued dissipation is introduced and compared with the scalar viscosity. The connection between this artificial viscosity and flux limiters is shown. Any flux limiter can be used as the basis of a shock detector for an artificial viscosity. We compare the use of the van Leer, van Albada, minmod, superbee, and the "average" flux limiters for this central difference scheme. For time dependent problems we need to use a small enough time step so that the CFL is less than one even though the scheme is linearly stable for larger time steps. Using a TVB Runge–Kutta scheme yields minor improvements in the accuracy.

1. BASIC SCHEME

The basic elements of the scalar dissipation model considered in this paper were first introduced by Jameson, Schmidt, and Turkel [2] using an explicit Runge–Kutta time integration scheme. The space discretization is based on central differences with an additional artificial viscosity. In this section the basic scheme is briefly reviewed.

Consider the Euler equations in the form

$$W_t + f_x = 0, \tag{1}$$

where W is the three-component vector of conserved variables, and f is the flux vector. The independent variables are time t and Cartesian coordinate x. In a cell-centered, finite-volume method, (1) is integrated over an elemental volume in the discretized computational domain. Equation (1) can also be written as

$$W_t + AW_x = 0,$$

where A is the flux Jacobian matrix defined by $A = \partial f/\partial W$.

To advance the scheme in time we use a multistage scheme. There are many ways of using Runge–Kutta schemes; a popular version is that of [2]. A typical step of this Runge–Kutta approximation to (1) is

$$W^{(k)} = W^{(0)} - \alpha_k \frac{\Delta t}{\Delta x}\left[Df^{(k-1)} - AV\right], \tag{2}$$

where D is the spatial differencing operator and AV represents the artificial dissipation terms. The derivatives of the fluxes are approximated by central differences. In the form presented here the scheme cannot have greater than second-order accuracy in time for nonlinear problems. For steady state problems the time accuracy is irrelevant and the form of (2) requires only two levels of storage. If one wishes to obtain higher accuracy in time for nonlinear problems, then one can use any formula from standard numerical ODE theory. In particular, the classcial Runge–Kutta scheme will give fourth-order accuracy using four stages but will require more storage than (2). It is shown in [9] that these schemes are TVD when the time dimension is continuous, i.e., a semi-discrete formulation. We will also consider Runge–Kutta forms that preserve the TVD nature of the semi-discrete version [6, 7]. In all cases, the spatial accuracy is determined only by the accuracy of the operator D to the derivative.

0021-9991/93 $5.00

The dissipation terms are a blending of second and fourth differences. That is,

$$AV = (D^2 - D^4)W,$$

where

$$D^2W = \Delta_-[(\lambda_{i+1/2}\epsilon^{(2)}_{i+1/2})\Delta_+]W_i, \tag{3}$$

$$D^4W = \Delta_-[(\lambda_{i+1/2}\epsilon^{(4)}_{i+1/2})\Delta_+\Delta_-\Delta_+]W_i, \tag{4}$$

and Δ_+, Δ_- are the standard forward and backward difference operators, respectively. The variable scaling factor λ is chosen as

$$\lambda_{i+1/2} = \tfrac{1}{2}[\lambda_i + \lambda_{i+1}], \tag{5}$$

where λ_i is proportional to the wave speed. The coefficients $\epsilon^{(2)}$ and $\epsilon^{(4)}$ are adapted to the flow and are defined as

$$\begin{aligned} \epsilon^{(2)}_{i+1/2} &= \kappa^{(2)} \max(\nu_i, \nu_{i+1}), \\ \epsilon^{(4)}_{i+1/2} &= \max[0, (\kappa^{(4)} - \varepsilon^{(2)}_{i+1/2})], \end{aligned} \tag{6}$$

where $\kappa^{(2)}$ and $\kappa^{(4)}$ are constants to be specified.

The parameter ν is a shock detector. We shall analyze ways of defining ν in detail in the next section. The purpose of this second difference viscosity is to introduce an entropy-like condition and to suppress oscillations in the neighborhood of shocks. Ideally the value of ν should be one at shocks and be negligible in smooth regions of the flow. The fourth-difference dissipation term is basically linear and is included to damp high-frequency modes and allow the scheme to approach a steady state. The second-order dissipation contains a nonlinear term which is of higher order in smooth regions. Hence, this term does not affect the linear stability of the scheme. Near shocks it is reduced to zero. For time dependent flows, the fourth-order dissipation is not very important and $\kappa^{(4)}$ will usually be small or zero.

2. SHOCK DETECTORS AND FLUX LIMITERS

In order to see the effect of ν we first define

$$\phi_i = 1 - \hat{\nu}_i. \tag{7}$$

A review of modern schemes with flux limiters is presented in [14] and hence we shall not go into great detail about flux limiters for upwind schemes. A comparison of such schemes for a scalar nonlinear problem is presented in [13]. As shown in [9] ϕ can be interpreted as a flux limiter, although its properties for central difference schemes is slightly different than for upwind schemes. The value of ϕ is usually taken as a function of r, where

$$r = \frac{u_i - u_{i-1}}{u_{i+1} - u_i} = \frac{\Delta_-}{\Delta_+}. \tag{8}$$

According to the TVD theory for a scalar equation in one dimension the artificial viscosity can sometimes be negative, see (21). However, for multidimensional vector equations with central differences we prefer to be conservative and choose the artificial viscosity, $\epsilon^{(2)}$, to be positive and so we set

$$\nu_i = |1 - \phi_{\text{central}}|. \tag{9}$$

Note, that in general $\hat{\nu} \neq \nu$. For the fluid dynamic equations we choose the pressure as a representative of the flow field. The artificial viscosity used in the original algorithm was

$$\nu_i = \left|\frac{p_{i+1} - 2p_i + p_{i-1}}{p_{i+1} + 2p_i + p_{i-1}}\right|, \tag{10}$$

and $\nu_{i+1/2} = \max(\nu_i, \nu_{i+1})$. We note that with this definition of ν that ϕ is not a function of r. We shall demonstrate in the result section that this switch gives rise to oscillations in the flow field.

In order to connect this artificial viscosity with flux limiters we first consider the van Leer flux limiter given by

$$\phi_i(r) = \frac{r + |r| + \varepsilon}{1 + |r| + \varepsilon}, \tag{11}$$

where ε is added to prevent the switch from being activated by noise. This ε is mainly needed for steady state calculations. Then after multiplying (11) by $|\Delta_+|$ we obtain

$$1 - \phi_i(r) = \frac{(\Delta_+ - \Delta_-)\operatorname{sgn}(\Delta_+)}{|\Delta_-| + |\Delta_+| + \varepsilon|\Delta_+|}. \tag{12}$$

Reverting back to the notation of pressure and modifying the ε term to remove $|\Delta_+|$ we obtain

$$\nu_i = |1 - \phi_i(r)| = \frac{|p_{i+1} - 2p_i + p_{i-1}|}{|p_{i+1} - p_i| + |p_i - p_{i-1}| + \varepsilon}, \tag{13}$$

For dimensional consistency we wish to choose ε to depend on the pressure. So we choose $\varepsilon = \epsilon(p_{i+1} + 2p_i + p_{i-1})$. Substituting this into (13) we obtain

$$\nu_i = \frac{|p_{i+1} - 2p_i + p_{i-1}|}{|p_{i+1} - p_i| + |p_i - p_{i-1}| + \epsilon(p_{i+1} + 2p_i + p_{i-1})}. \tag{14}$$

There is no special need to base the artificial viscosity on the van Leer flux limiter. It is just coincidental that the resultant viscosity v closely resembles the original artificial viscosity, (10). Another alternative is the van Albada flux limiter,

$$\phi_i(r) = \frac{r + |r|}{1 + r^2}, \tag{15}$$

We note that this limiter approaches zero for large values of r, while most limiters approach two as r increases. Using a similar derivation we find that the artificial viscosity associated with the van Albada limiter is given by

$$v_i = \frac{\begin{pmatrix}(p_{i+1}-p_i)^2 + (p_i - p_{i-1})^2 - (p_{i+1}-p_i) \\ \times (p_i - p_{i-1}) - |(p_{i+1}-p_i)(p_i - p_{i-1})|\end{pmatrix}}{\begin{pmatrix}(p_{i+1}-p_i)^2 + (p_i - p_{i-1})^2 \\ + \epsilon(p_{i+1} + 2p_i + p_{i-1})^2\end{pmatrix}}. \tag{16}$$

There is a second version of the van Albada flux limiter used in the literature,

$$\phi_i(r) = \frac{r + r^2}{1 + r^2}, \qquad 0 \leqslant r \leqslant 1. \tag{17}$$

Others limiters used are minmod,

$$\phi_i(r) = \max(\min(r, 1), 0),$$

and superbee

$$\phi_i(r) = \max(\min(2r, 1), \min(r, 2), 0);$$

see [10]. We shall also consider the "average" flux limiter

$$\phi_i(r) = \text{minmod}((1 + r)/2, 2\ \text{minmod}(1, r)).$$

For each of these limiters there is a corresponding "artificial" viscosity.

For an upwind flux limiter we have $\phi(1/r) = (1/r)\,\phi(r)$. Huynh [1] has shown that the resultant scheme is second order if $\phi'(1) = \frac{1}{2}$. By (9) the effective ϕ_{central} satisfies $0 \leqslant \phi \leqslant 1$ so that the artificial viscosity v is positive. Note that for upwind schemes v by (7) can be negative whenever doing so does not destroy the TVD properties. This can have both advantages and disadvantages. Upwind schemes tend to have less dissipation, especially on coarse meshes, than central difference schemes even with a matrix viscosity because of this "anti-viscosity." On the other hand, central difference schemes frequently converge faster to a steady state because v is always positive. Combining (7) and (9) we have

$$\phi_{\text{central}} = \begin{cases} \phi_i & \text{if } \phi < 1, \quad r < 1 \\ 2 - \phi_i & \text{if } \phi > 1, \quad r > 1 \end{cases}$$

With the van Leer and first Van Albada flux limiters one finds that $\phi(1/r) = \phi(r)$; i.e., it does not make any difference in (8) if r is a forward difference over a backward difference or a backward difference over a forward difference. For smoothness we now want $\phi'(1) = 0$. Of the above limiters only the first version of Van Albada and superbee have this property. This property gives a local second-order accuracy. When the accuracy is only first order at shocks it still is not known how this contaminates the global accuracy of the approximation. It follows from the analysis of [1] that an upwind scheme can be considered as a symmetric interpolation followed by a upwind convection operator. A central difference scheme can be represented as a downwind interpolation followed by a compensating upwind convection and so the total operation is symmetric.

3. THE TVD PROPERTY

Consider the one-dimensional scalar conservation law

$$\frac{\partial}{\partial t}[u(x, t)] + \frac{\partial}{\partial x}[f(u(x, t))] = 0, \tag{18}$$

where

$$-\infty < x < \infty, \qquad t \geqslant 0.$$

Let $v(t) = \{v_j(t)\}$ be the approximation solution of (18) and consider the semidiscrete equation

$$\frac{d}{dt} v_i(t) + \frac{1}{2\Delta x}[f_{i+1} - f_{i-1}]$$
$$= \frac{1}{2\Delta x}[Q_{i+1/2}, \Delta v_{i+1/2} - Q_{i-1/2}\,\Delta v_{i-1/2}]$$
$$- \frac{\kappa^{(4)}}{\Delta x}[R_{i+1/2}\Delta^3 v_{i+1/2} - R_{i-1/2}\Delta^3 v_{i-1/2}] \tag{19}$$

with

$$\Delta v_{i+1/2} = (\Delta v)_{i+1/2} = v_{i+1}(t) - v_i(t).$$

Δ^3 is a third-difference operator defined as

$$\Delta^3 v_{i+1/2} = v_{i+2}(t) - 3v_{i+1}(t) + 3v_i(t) - v_{i-1}(t).$$

The terms on the right-hand side of (19) represent second- and fourth-difference numerical dissipation terms, with $\kappa^{(4)}$ a constant. Define

$$s_{i+1/2} = \operatorname{sgn}(\Delta v_{i+1/2}),$$

where sgn represents the signum function. We first shift the indices by one in (19) and subtract (19) from the resulting equation. We then multiply the result by $s_{i+1/2}$ and sum over all i. Noting that $s_{i+1/2} = \pm 1$, so $s_{i+1/2}^2 = 1$, and

$$s_{i+1/2}\,\Delta v_{i+1/2} = |\Delta v_{i+1/2}|.$$

Let TV denote the total variation as given by

$$\mathrm{TV} = \sum_i |\Delta v_{i+1/2}|.$$

We then obtain

$$\begin{aligned}
\frac{d}{dt}\sum_i |\Delta v_{i+1/2}| &= -\frac{1}{2\Delta x}\sum_i s_{i+1/2}(s_{i-1/2} - s_{i+3/2})\frac{\Delta f_{i+1/2}}{\Delta v_{i+1/2}}|\Delta v_{i+1/2}| \\
&\quad + \frac{1}{2\Delta x}\sum_i s_{i+1/2}(s_{i+3/2} - 2s_{i+1/2} + s_{i-1/2}) \\
&\quad \times Q_{i+1/2}\,|\Delta v_{i+1/2}| \\
&\quad - \frac{\kappa^{(4)}}{\Delta x}\sum_i (s_{i+3/2} - 2s_{i+1/2} + s_{i-1/2}) \\
&\quad \times R_{i+1/2}\Delta^3 v_{i+1/2}.
\end{aligned}$$

We stress that the last term will not help for TVD. Its purpose is to eliminate high frequencies and accelerate convergence to a steady state. Hence, we want this contribution to be zero. This can be accomplished if we demand either

$$s_{i+3/2} - 2s_{i+1/2} + s_{i-1/2} = 0$$

or

$$R_{i+1/2} = 0.$$

We are then left with

$$\begin{aligned}
\frac{d}{dt}(\mathrm{TV}) = -\frac{1}{2\Delta x}\sum_i &- s_{i+1/2}(s_{i+3/2} - s_{i-1/2}) \\
&\times \frac{\Delta f_{i+1/2}}{\Delta v_{i+1/2}}|\Delta v_{i+1/2}| \\
&- s_{i+1/2}(s_{i+3/2} - 2s_{i+1/2} + s_{i-1/2}) \\
&\times Q_{i+1/2}\,|\Delta v_{i+1/2}|. \qquad (20)
\end{aligned}$$

Thus, a sufficient condition that the total variation not increase is that each term in the summation of (20) must be positive. This means that the scheme is TVD if

$$\begin{aligned}
&-s_{i+1/2}(s_{i+3/2} - 2s_{i+1/2} + s_{i-1/2})\,Q_{i+1/2} \\
&\quad \geqslant s_{i+1/2}(s_{i+3/2} - s_{i-1/2})\frac{\Delta f_{i+1/2}}{\Delta v_{i+1/2}}. \qquad (21)
\end{aligned}$$

This is the inequality obtained in [9].

When driving the solution to a steady state one frequently finds that it is not advantageous for the scheme to be TVD. The reason is, that with TVD schemes the switches are frequently being turned on and off due to local noise. For steady state calculations this causes the convergence to halt at some error level and a limit cycle results in which the residual oscillates about some level instead of decreasing. To prevent this from occurring we wish to prevent the switch from being activated for small oscillations or small discontinuities. The inequality (21) was obtained by demanding that the solution be TVD and so each term on the right-hand side of (20) was negative independent of the size of $\Delta f_{i+1/2}/\Delta v_{i+1/2}$. Instead we shall only demand that the solution be total variation bounded (TVB). Now, each term on the right-hand side of (20) can be positive as long as it is bounded by a constant times $|\Delta v_{i+1/2}|$. This is valid for $0 \leqslant t \leqslant T$. In theory this can prevent a steady state from being reached as $t \to \infty$. However, if the steady state is reached then the solution is well behaved. Since $s_{i+1/2}$ is equal to plus or minus one we want

$$-Q_{i+1/2} + \frac{\Delta f_{i+1/2}}{\Delta v_{i+1/2}} < \alpha \qquad (22)$$

for some constant α.

We shall choose

$$Q_{i+1/2} = v_{i+1/2}\left|\frac{\Delta f_{i+1/2}}{\Delta v_{i+1/2}}\right|. \qquad (23)$$

This is similar to (5), (6) with $\kappa^{(2)} = \frac{1}{2}$, $v_{i+1/2} = \max(v_i, v_{i+1})$, and $\lambda = \Delta f_{i+1/2}/\Delta v_{i+1/2}$. We then rewrite (23) as

$$(1 - v_{i+1/2})\frac{\Delta f_{i+1/2}}{\Delta v_{i+1/2}} < \alpha. \qquad (24)$$

Equation (24) demands a bound on the multiplication of $1 - v$ with $\Delta f/\Delta v$. Hence, if $\Delta f/\Delta v$ is small then we can allow v to be small. Only if $\Delta f/\Delta v$ is large do we need $v \to 1$. We choose v to depend on the strength of the shock, Δv. For weak shocks Δv is small and we can choose ϵ in (14) near one. For strong shocks Δv is large, so we want ϵ to be small

to make v a TVD switch. For the fluid dynamic equations we replace the vector v by the scalar pressure, p.

To find such a v we use (14). When $\epsilon = 0$ we obtain the TVD switch (14) while with $\epsilon = 1$ we obtain a perturbation of the original switch, (10) for transonic flows. This switch treats the two sides of the shock asymmetrically depending on whether p_i is to the left or right of the shock. Thus, we replace it by

$$v_i = \frac{|p_{i+1} - 2p_i + p_{i-1}|}{|p_{i+1} - p_i| + |p_i - p_{i-1}| + \epsilon \max(p_{i+1}, p_i, p_{i-1})}.$$

In practice the switch that we use is

$$v_i = \frac{|p_{i+1} - 2p_i + p_{i-1}|}{\begin{pmatrix}(1-\epsilon)(|p_{i+1} - p_i| + |p_i - p_{i-1}|)\\ +\epsilon(p_{i+1} + 2p_i + p_{i-1})\end{pmatrix}}. \tag{25}$$

We wish to choose ϵ automatically based on the shock strength. One possibility for ϵ is

$$\epsilon_i = \left\{\frac{\min(p_{i-2}, p_{i-1}, p_i, p_{i+1}, p_{i-2})}{\max(p_{i-2}, p_{i-1}, p_i, p_{i+1}, p_{i-2})}\right\}^{\sigma}, \tag{26}$$

where σ is a free parameter. A reasonable range is $\sigma = \frac{1}{2}$ to $\sigma = 1$.

For small oscillations p_i does not vary much and so ϵ is slightly less than one. For large oscillations ϵ is equal to the relative jump across the shock. Consider a perfectly resolved discontinuity going from p_L to p_R with $p_R < p_L$. Then,

$$v = \frac{p_L - p_R}{(p_L - p_R) + \epsilon p_L}, \qquad \varepsilon = \left\{\frac{p_R}{p_L}\right\}^{\sigma}. \tag{27}$$

Let

$$q = \frac{p_R}{p_L}.$$

Combining these we find that

$$v = \frac{1}{1 + q^{\sigma}/(1-q)}.$$

Hence, for small q (i.e., for large discontinuities) $v \sim 1 - q^{\sigma}$. Hence for both very weak shocks and very strong shocks the left-hand side of (24) is small, i.e., $(1-v)\,\Delta v \to 0$ as $\Delta v \to 0$ and also as $\Delta v \to \infty$. This discussion has concentrated on the theoretical basis of the algorithm. In practice the formula (25) is used for transonic, supersonic, and hypersonic flow regimes.

In this section we have written the flux limiters and artificial viscosity in terms of the pressure variable which is appropriate for inviscid fluid dynamics. In the next section we shall consider matrix viscosities. With a matrix viscosity one can base the limiter in each characteristic field on a different quantity.

4. MATRIX VISCOSITY

In the above discussion we have discussed a scalar equation. In the original algorithm, this procedure was applied to each equation with the same ϵ. The coefficient λ in (5) was chosen as equal to the spectral radius $|u| + c$ while v was the same switch that depended on the pressure, for all the equations. For time dependent flows this presents several difficulties, first as seen in the result section there is excessive smearing since the same coefficient is used for all waves and is proportional to the fastest wave speed. Second, pressure is continuous across a contact discontinuity and so a pressure based switch will not sense a contact. We therefore replace the scalar dissipation with a matrix dissipation, i.e., λ in (3.4) is now a matrix-valued function. We first define a function of a matrix A. We assume that A can be diagonalized so that TAT^{-1} is diagonal. We wish to introduce the absolute value of the matrix A in a way which is computationally efficient. We consider the form of TDT^{-1} for an arbitrary diagonal matrix D where the columns of T^{-1} are the eigenvectors of A, the coefficient of the x derivative in the PDE. We see that certain patterns reappear in this form. We are then led to define our function as

$$f(A) = \lambda_3 I + \left(\frac{\lambda_1 + \lambda_2}{2} - \lambda_3\right)\left[\frac{\gamma - 1}{c^2} E_1 + E_2\right] + \frac{\lambda_1 - \lambda_2}{2c}\left[E_3 + (\gamma - 1)\, E_4\right], \tag{28}$$

where

$$E_1 = \begin{pmatrix} \frac{u^2}{2} & -u & 1 \\ \frac{u^3}{2} & -u^2 & u \\ \frac{Hu^2}{2} & -uH & H \end{pmatrix},$$

$$E_2 = \begin{pmatrix} 0 & 0 & 0 \\ -u & 1 & 0 \\ -u^2 & -u & 0 \end{pmatrix},$$

$$E_3 = \begin{pmatrix} -u & 1 & 0 \\ -u^2 & u & 0 \\ -uH & H & 0 \end{pmatrix},$$

$$E_4 = \begin{pmatrix} 0 & 0 & 0 \\ u^2 & -u & 1 \\ \frac{u^3}{2} & -u^2 & u \end{pmatrix}.$$

Whenever the matrix A can be diagonalized, i.e., $D = T^{-1}AT$ is diagonal then a function of the matrix is defined by $f(A) = Tf(D)\,T^{-1}$, and $f(D)$ is the function f applied to each element of the diagonal of D. Let the coefficients λ_1, λ_2, and λ_3 be functions of the eigenvalues of A. If $\lambda_1 = u + c$, $\lambda_2 = u - c$, $\lambda_3 = u$, then we recover the matrix A. When the λ's are the absolute value of the eigenvalues we obtain the absolute value of the matrix A. In general, λ_1, λ_2, and λ_3 should not be exactly equal to the eigenvalues of A since at sonic points or stagnation points an eigenvalue is zero and hence no artificial viscosity would be added. Hence, the λ's have a lower limit of $0.2\,|u + c|$. This procedure also allows one to select different switches for each eigenvalue. In particular we shall base the switch for the nonlinear fields, with speeds λ_1 and λ_2 on the pressure. However, the pressure is continuous across a contact discontinuity. Hence, the switch for the linear field, λ_3 is based on the temperature, $T = p/\rho$. Putting these options together we choose the λ's equal to $\epsilon^{(2)}$ and $\epsilon^{(4)}$ times the limited absolute value of the eigenvalues, see (3, 4).

5. RESULTS

The results were all obtained using a multistage Runge–Kutta scheme (2) to advance the solution in time. For most of the computational results the original Runge–Kutta coefficients [2] were used, $\alpha_1 = \frac{1}{4}$, $\alpha_2 = \frac{1}{3}$, $\alpha_3 = \frac{1}{2}$, $\alpha_4 = 1$. Shu [6] introduced another set of coefficients to guarantee that the scheme is TVD in time but is only first-order accurate. The three stage scheme has coefficients, $\alpha_1 = \frac{1}{9}$, $\alpha_2 = \frac{1}{3}$, $\alpha_3 = 1$ while the four-stage scheme has coefficients, $\alpha_1 = \frac{1}{16}$, $\alpha_2 = \frac{1}{6}$, $\alpha_3 = \frac{3}{8}$, $\alpha_4 = 1$. The more stages that are used the larger the time step allowed by stability requirements. However, we found that using larger time steps introduced oscillations into the solution. In practice we chose CFL = 0.75, and so there was no advantage to using the four stage scheme. Shu [7] also introduced higher order schemes for time dependent equations that are still TVB. These schemes can no longer be written in the simple form of (2). Instead each stage requires the use of the dependent variables and fluxes at previous stages and so more information needs to be stored.

We solve the one-dimensional Euler equations in the domain $0 \leqslant x \leqslant 10$. The initial conditions are $u = 0$ m/s, $T = 300$ K everywhere. The initial pressure is discontinuous with a ratio of $p = 20$ for $0 \leqslant x \leqslant 5$ to 1 for $5 \leqslant x \leqslant 10$. The density and total energy are then calculated from the ideal gas law with $\gamma = 1.4$.

We first consider the standard central difference algorithm with a scalar viscosity and the original switch (10) and the original Runge–Kutta coefficients with CFL = 0.75. The first figure is a plot of density as a function of x at a nondimensional time of 0.2. Large oscillations appear both between the rarefaction wave and the contact discontinuity and between the contact and the shock. We also considered the case that the switch (10) is based on density rather than pressure. This does not make any basic change in the results shown in Fig. 1. In Fig. 2 the density is plotted with the standard switch replaced by the van Leer-based switch (9, 11). The change in the switch has eliminated all oscillations since the scheme is TVD for the scalar case with this switch [9]. There are still some small oscillations in the rarefaction and the contact is very smeared. In Fig. 3 we show the same case using the matrix viscosity and $\epsilon = 0.008$. The switch for the nonlinear waves is based on the pressure as before. Since the pressure is continuous across a contact discontinuity, the switch for the entropy wave is based on the temperature; although one could also use entropy. We see from this figure that the smearing near the contact is considerably reduced. Figure 3 was based on the shock detector (12). We obtained similar results when the forward difference multiplying ε was replaced by a central difference. In practice we usually use (25). This requires the use of a much smaller ε to achieve similar results. All these test cases use a pressure based switch for the acoustic waves and a temperature based switch for the entropy and shear waves. When one or both of these switches are based on the density no noticeable differences are seen in the solution. For boundary layers there should be a difference between pressure based and density based switches. Also for isothermal boundary conditions there is a sharp gradient in the

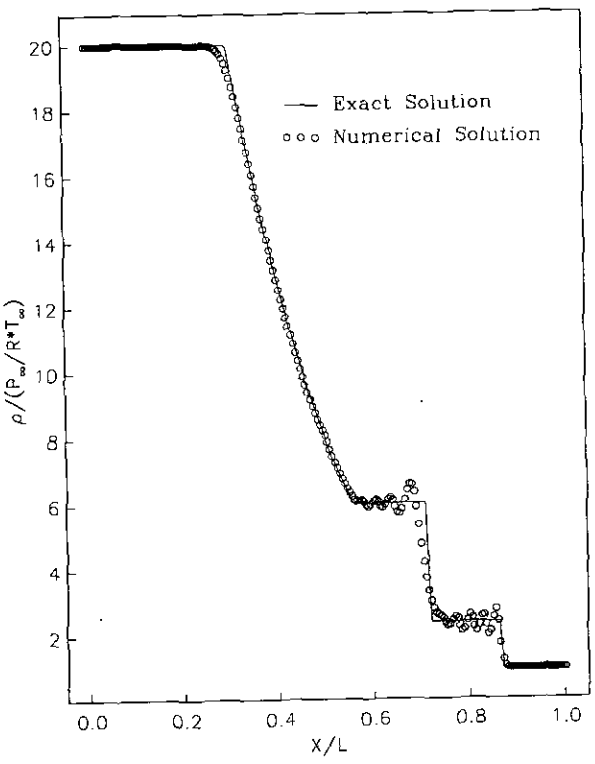

FIG. 1. Scalar viscosity with original switch.

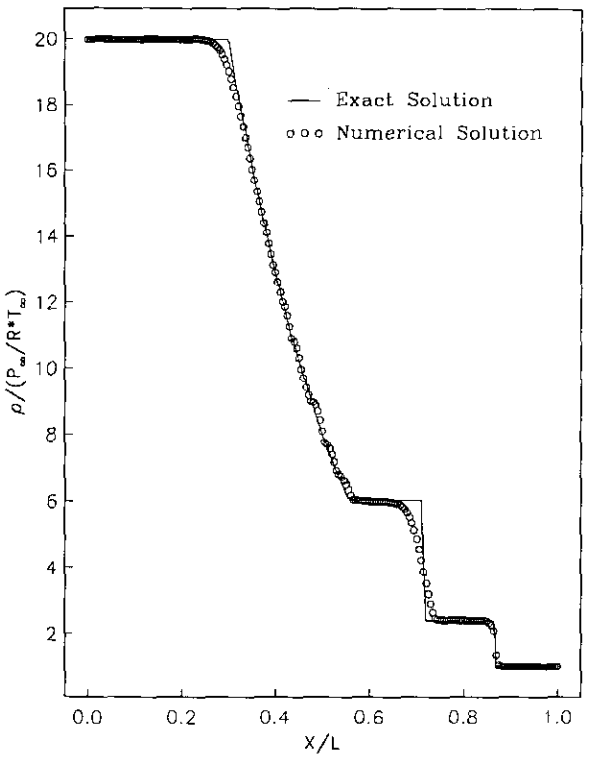

FIG. 2. Scalar viscosity with van Leer based switch.

temperature near the wall and a temperature based switch may be turned on even in the absence of any shocks.

Using the van Albada (1) based switch improves the treatment of the sonic point. The use of superbee for the nonlinear wave introduced new oscillations as seen in Fig. 4. This may be due to the fact that the superbee flux limiter is "overcompressive" and so its use on the nonlinear fields might create nonentropy satisfying shocks. For the linear field this "overcompression" can only steepen the discontinuity. We conclude, that for the central difference schemes superbee should never be used for the nonlinear waves. The results with minmod was similar to the van Leer viscosity but with a slightly less sharp shock. In all cases the head of the rarefaction wave was smeared out. In Fig. 5 we present the density when superbee is used for the linear wave while van Albada (1) is used for the nonlinear waves. We also used these schemes with the ϵ as given in (11). For the van Leer limiter we could choose $\epsilon = 0.1$ without significantly degrading the results while for van Albada (1) we had to choose ϵ about 0.005. For the steady problems we can use the van Leer limiter with $\epsilon = 0.1$ and still get monotone profiles. All the cases presented evaluate the artificial viscosity after the first stage and then freeze it for the later stages. If one reevaluates the artificial viscosity after each stage then a large undershoot at the foot of the expansion wave is introduced and there are increased difficulties at the sonic point.

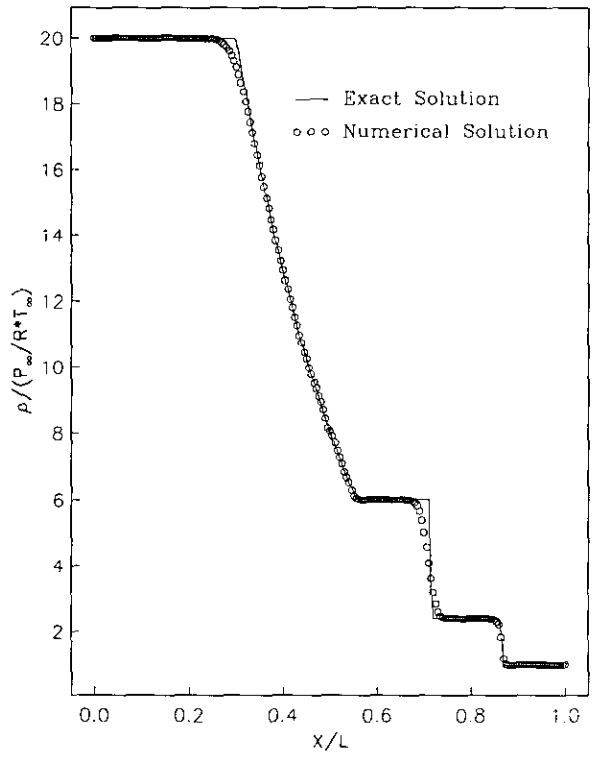

FIG. 3. Matrix viscosity with van Leer based switch.

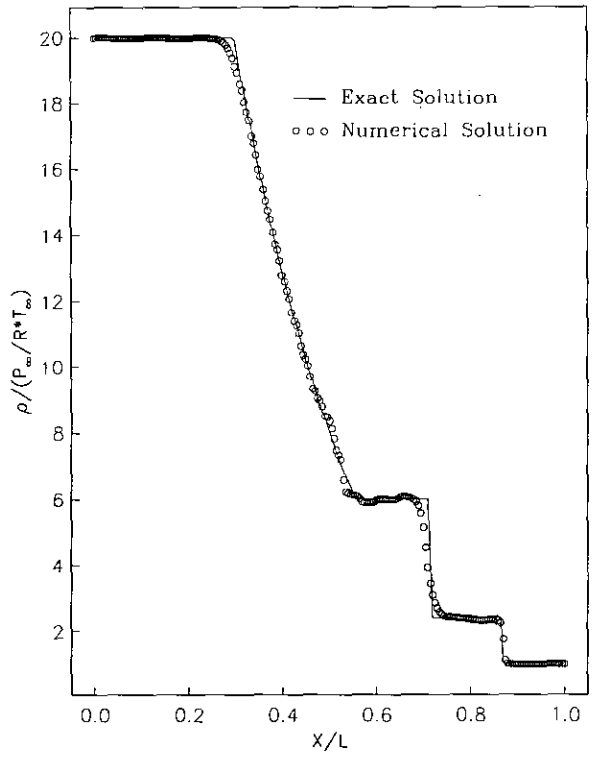

FIG. 4. Matrix viscosity with van Albada limiter for the linear wave and superbee for the nonlinear waves.

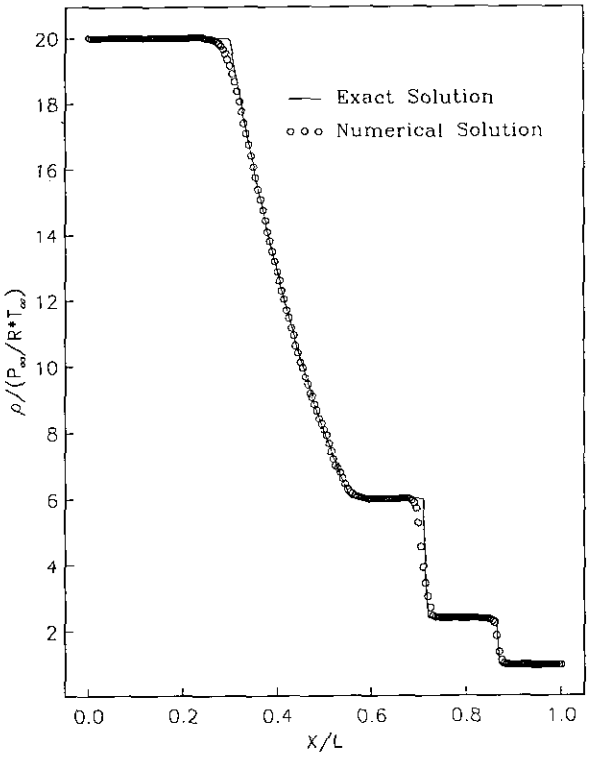

FIG. 5. Matrix viscosity with superbee for the linear wave and van Albada for the nonlinear waves.

The cases presented until now were with the original four stage Runge–Kutta coefficients and CFL = 0.75. Raising the CFL number introduced oscillations. We next tried the first-order scheme suggested by Shu [7] but still got oscillations when the CFL was larger than one. We then used the third-order Runge–Kutta scheme suggested by Shu [6]. Using the same switches for both the linear and nonlinear switches and these third-order Runge–Kutta coefficients resulted in a sharper profile but some oscillations. Hence, in Fig. 6 we present the results for Shu's third-order scheme in time, using superbee for the linear field and the van Leer viscosity for the nonlinear field. Figure 7 presents the same case as Fig. 6 but with the CFL raised to 0.95. This introduced a small oscillation near the sonic point but otherwise was very satisfactory. For all these cases the artificial viscosity was frozen after the first stage. It is interesting to note that with the scheme of Lerat and Sides [4] the solution becomes less oscillatory as the time step is increased. In our last case we consider the effect of using different variables for the switches. Until now the switch for the nonlinear fields has been based on the pressure while the switch for the linear field has been based on the temperature. We now plot the results when each characteristic field has an artificial viscosity switch based on that characteristic variable. In Fig. 8 the density is plotted for this case using Shu's third order Runge–Kutta coefficients, CFL = 0.75, the superbee limiter for the contact discontinuity based on the linearized

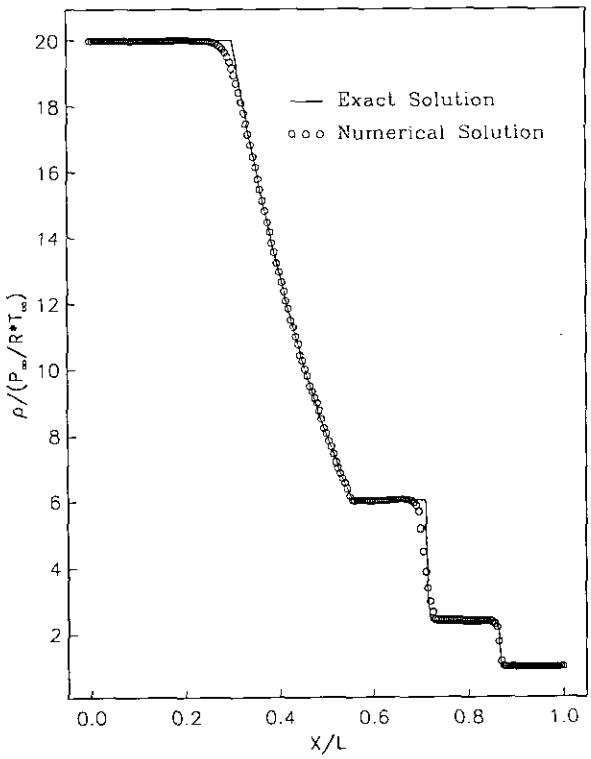

FIG. 6. Shu's third-order scheme with superbee limiter for the linear wave and van Leer limiter for the nonlinear waves, CFL = 0.75.

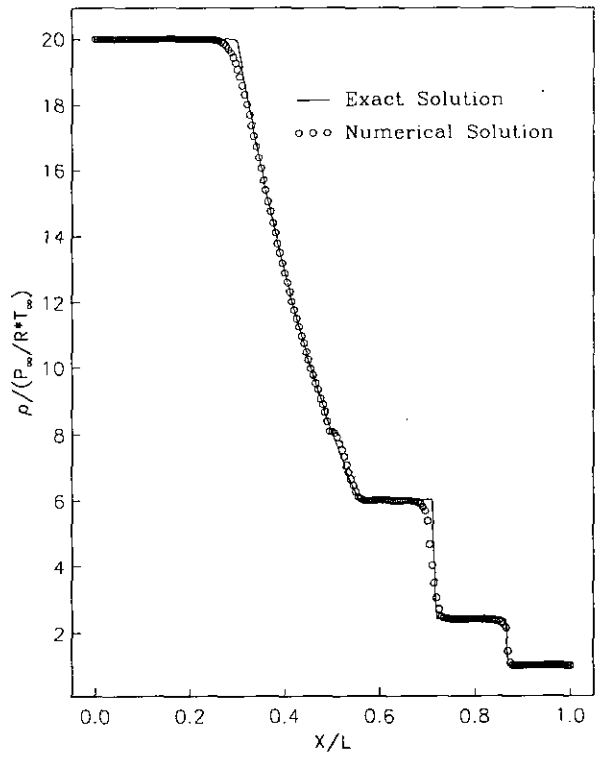

FIG. 7. Shu's third-order scheme with superbee limiter for the linear wave and van Leer limiter for the nonlinear waves, CFL = 0.95.

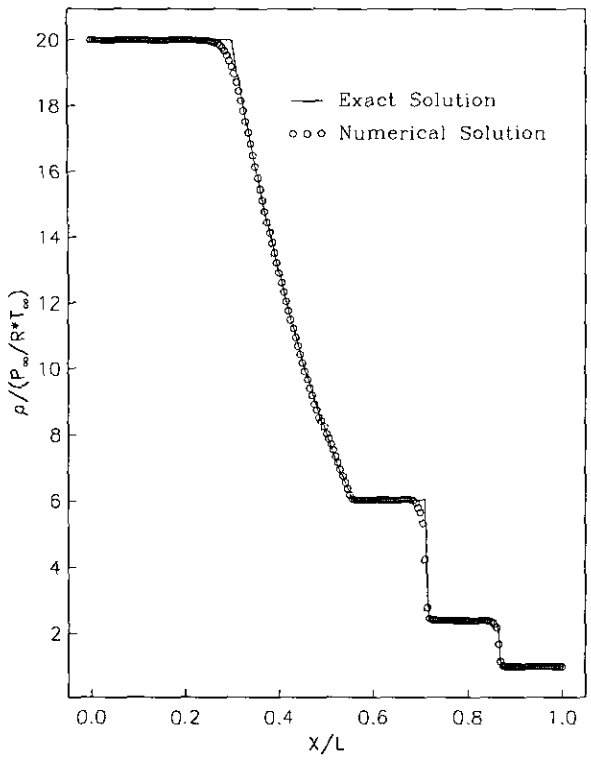

FIG. 8. Shu's third-order scheme with superbee limiter for the linear wave and van Leer limiter for the nonlinear waves based on characteristic variables.

entropy variable $\Delta p - c^2 \Delta \rho$, and the van Leer limiter for the acoustic variables $\Delta p + \rho c \Delta u$ and $\Delta p - \rho c \Delta u$. We see that there is an additional improvement in the resolution of the contact discontinuity. Here the artificial viscosity was frozen after the first stage. The evaluation of the artificial viscosity at each stage made only minor improvements in the solution compared to the large effect observed using the van Leer limiter with the standard Runge–Kutta scheme.

The solutions presented are all for the time $t = 0.2$. Watching the time evolution one sees that there are many oscillations that occur in the initial breakup of the discontinuity into a shock and a contact. These oscillations disappear as the solution progresses. All the calculations were done with a time step based on the largest eigenvalue at the previous time step. Hence, Δt varies at each time level. The result is that the time step in the initial stages of problem is approximately twice as large as those allowed after the transient has passed. If one uses a constant time step based on the long time behavior of the solution then there is a minor improvement at the sonic point.

We finally consider steady state two-dimensional calculations. We use multigrid as an acceleration technique to reach a steady state faster [3]. In all cases we use a FMG version of multigrid. There are two levels of refinement meshes beneath the finest mesh to obtain a good starting condition. Within each mesh a W cycle is used with one iteration on the finest mesh and two iterations of the Runge–Kutta smoother on all coarser meshes. For the high speed flows the first 100 iterations on the coarsest refinement mesh is done without any multigrid and a small CFL number. The convergence plots show the residual for the three grids. Whenever the solution is interpolated to the next finest grid the residual jumps up.

We first solve for the turbulent flow about a blunt cone using a Baldwin–Lomax turbulence model at $M_\infty = 25.0$, $\alpha = 0$. The grid is 400×80 and the geometry is shown in Fig. 9a. In Fig. 9b we plot the pressure and Mach number along the coordinate line directly in front of the cone. We choose $\epsilon = 0.05$ in (25). There are only three points in the shock and no overshoots even at this hypersonic speed. If ϵ is chosen equal to one (i.e., original switch (10)) the code does not converge. In Fig. 9c we plot the pressure and Mach number along the leading edge coordinate line but now with $\epsilon = 0.90$. The results are similar to that previously obtained but now the upper portion of the shock is rounded. We also need a larger value of the second and fourth difference dissipation for the algorithm to converge to the steady state. In Fig. 9e we present the same plot when the Van Albada (1) switch is used. The sharpness of the shock is similar to the previous result but the convergence is slowed down. This seems to be happen because the second difference viscosity is now turned on only right near the shock.

We next consider laminar transonic flow about a NACA0012 with $M_\infty = 0.8$, $\alpha = 1.0$. In Figs. 10a and 10b we plot C_p with $\epsilon = 0.05$ and $\epsilon = 1.00$, respectively. We note that the "TVD" solution $\epsilon = 0.05$ has completely smeared the solution, i.e., a TVD-like switch adds too much viscosity at the weak shock. The solution to this difficulty is to make the switch depend on the strength of the discontinuity as advocated in (26), (27). For the following runs we chose $\sigma = \frac{1}{2}$. In Fig. 10c we plot C_p with this variable ϵ and we see that we recover the $\epsilon = 1.0$ results. To further improve the quality of the results we use the matrix viscosity and these results plotted in Fig. 10d show a much sharper shock. When using a small variable of ϵ the shock is still smeared even with the matrix viscosity. To demonstrate that we still can handle the strong shock case we redo the blunt body case done above with the same variable ϵ. In Fig. 9d we plot the same pressure and Mach levels and note that we obtain the same sharp profile as Fig. 9b. Hence, the variable ϵ does choose the appropriate amount of dissipation for both transonic and hypersonic flows. In Figs. 9f and 10e, 10f we show the convergence rate of ρ for the hypersonic and transonic cases respectively.

The matrix viscosity adds approximately 20% to the total computer time needed to advance one time step. For time dependent problems this is the total cost of the matrix viscosity. However, for the steady state problems the decreased viscosity inherent in the matrix form also slows down the convergence to a steady state. The amount of

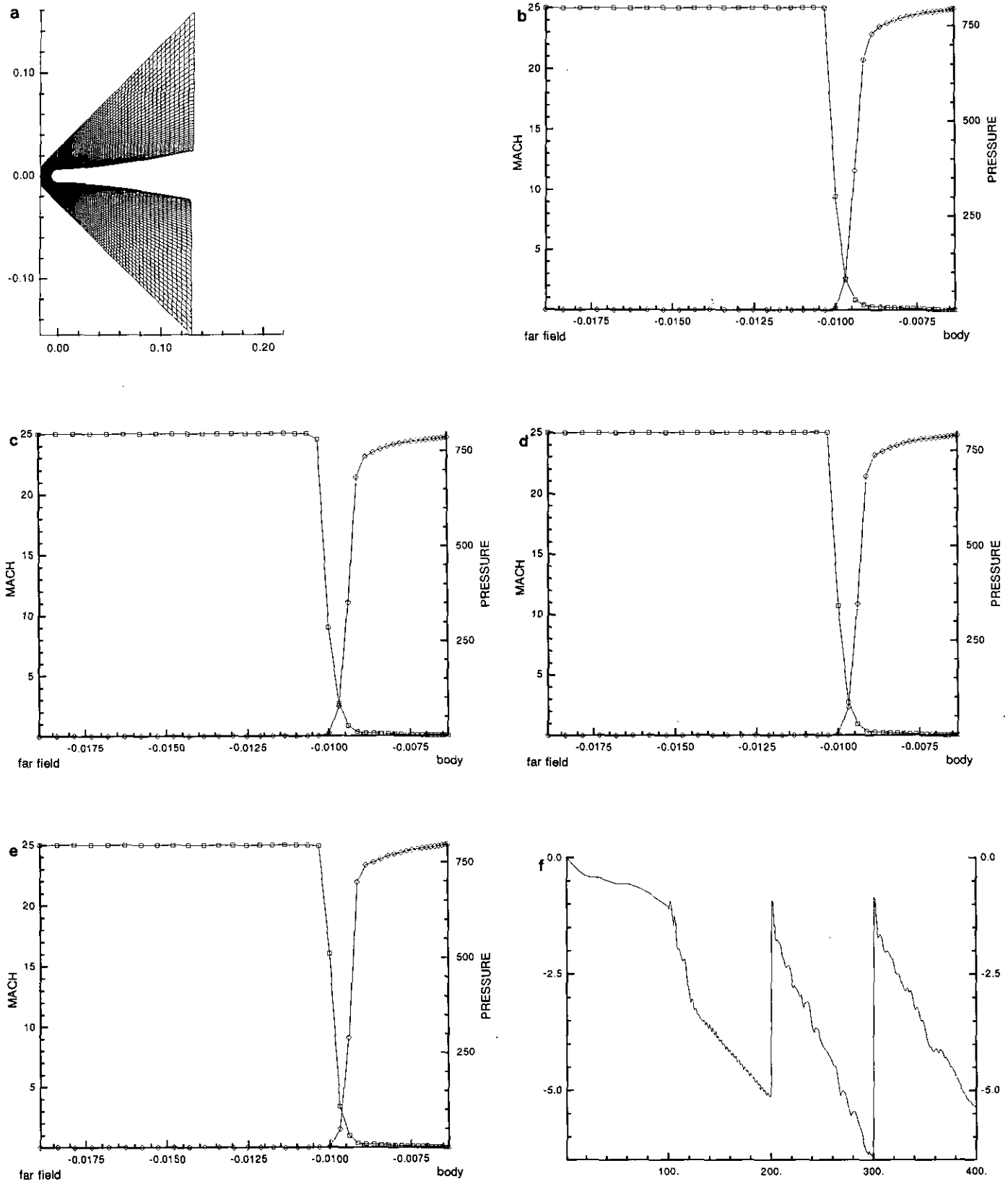

FIG. 9. (a) Geometry for blunt cone; (b) MACH = 25.0, $\varepsilon = 0.05$; (c) MACH = 25.0, $\varepsilon = 0.90$; (d) MACH = 25.0, variable (sqrt)ε; (e) MACH = 25.0, van Albada (1) Switch, $\varepsilon = 0.05$; (f) convergence history, 200, 100, 100 cycles on three grids, variable ε.

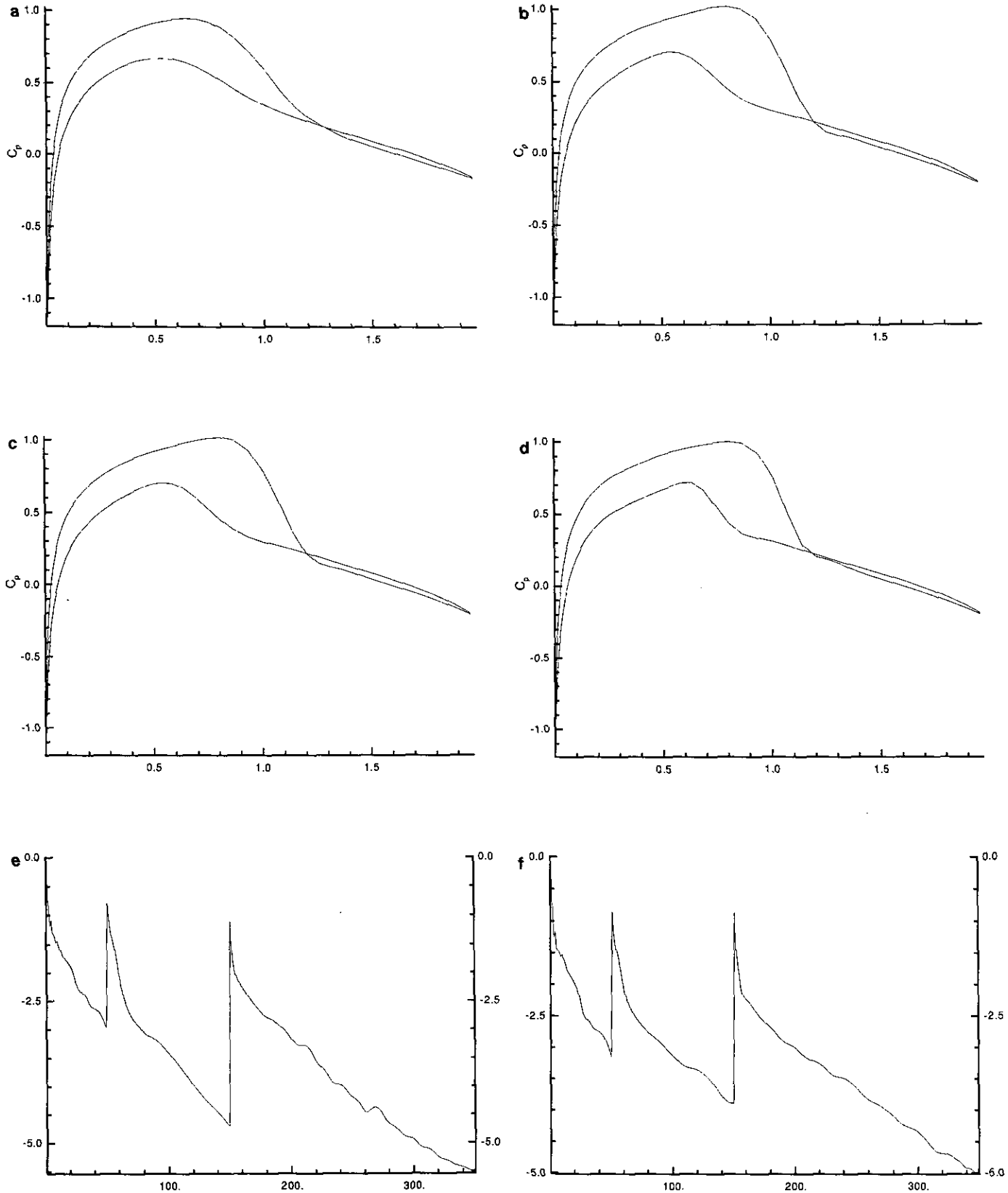

FIG. 10. NACA0012: (a) MACH = 0.80, $\alpha = 1.0$, $\varepsilon = 0.05$; (b) MACH = 0.80, $\alpha = 1.0$, $\varepsilon = 1.0$; (c) MACH = 0.80, $\alpha = 1.0$, variable (sqrt)ε; (d) MACH = 0.8, $\alpha = 1.0$, matrix viscosity, variable ε. Convergence history, 50, 100, 200 cycles on three grids; (e) $\varepsilon = 1.0$; (f) matrix viscosity, variable ε.

degradation is problem dependent but typically one needs about 20% more iterations to reach the same residual level. Hence, the total cost of the matrix viscosity is about 40 to 45% for steady state problems. Nevertheless, the matrix viscosity is still cheaper than most upwind codes. Further comparisons depend on the details of the upwind code and the programming aspects. Other examples are presented in [9].

We again stress that for the hypersonic cases the value of ϵ chosen essentially makes the algorithm TVD (in the one-dimensional scalar sense). However, for the transonic case the appropriate value of ϵ gives an artificial viscosity well below that required for a TVD scheme. This demonstrates that the coefficient of the artificial viscosity or equivalently the flux limiter should depend on the strength of the discontinuity, at least for steady calculations.

6. CONCLUSION

- The use of a matrix viscosity allows a central difference scheme to behave similar to an upwind scheme. By using the above forms one need not calculate the characteristic variables and instead one can multiply $|A|$ times a vector efficiently. This has the disadvantage that the switches, or flux limiters, cannot easily be based on the characteristic variables. Instead they are based on physical variables as pressure or temperature. This makes the choice "physical" rather than mathematical. More testing is needed to compare these choices. In most other ways the flux difference splitting and central differencing with matrix viscosity are similar. On historical grounds upwind schemes are frequently coupled with an implicit solver while central difference schemes are advanced with a multistage scheme with a multigrid acceleration. However, this is not an essential difference. Flux difference schemes can have difficulties with slow moving shocks or the "carbuncle phenomena" and some of the fixes involve adding dissipation to the upwind scheme (see [5]). Hence, these upwind schemes frequently involve many of the same fixes and choice of flux limiters that are implemented in central difference schemes.

- Hence, using a central difference scheme with an artificial viscosity we can duplicate most of the accuracy of upwind TVD schemes. Solving the one-dimensional time dependent Euler equations we obtain high resolution solutions for the shocks and the contact discontinuity. The main ingredients are an improved shock locator and a matrix artificial viscosity. This shock locator can be based on any of the upwind flux limiters. Superbee is the best for the contact while either van Leer or van Albada (1) is best for the nonlinear waves. Further minor improvements can be obtained by using a high order TVD Runge–Kutta scheme and basing the switch on the characteristic variables. The TVB Runge–Kutta schemes is slightly more accurate than the standard Runge–Kutta schemes.

- There are major differences between the time dependent problem and the steady state problem. For the time dependent problem it was necessary for the scheme to be TVD-like in order to avoid oscillations. However, for the steady state problem we use a coefficient for the artificial viscosity that is considerably below that required for the solution to be TVD and still obtain monotone shocks, especially if the shock is not very strong. Even for $M_\infty = 25.0$ there are only three points in the shock. TVD schemes frequently slow down the convergence to the steady state unless the flux limiters are carefully constructed. When using a TVD scheme coupled with a multigrid acceleration it may be necessary to limit the transfer of the residual to coarser meshes in the vicinity of shocks. Hence, there is a need for more work to extend the TVD theory to steady state problems and weak shocks.

- For time dependent flows we were not able to use a CFL greater than one, even though the linear stability of the Runge–Kutta allowed larger time steps. For the steady state problems one can use larger time steps. Hence, for steady-state problems it is efficient to use many stages in the Runge–Kutta method to increase the CFL stability limit even though one is not interested in high time accuracy. Nevertheless, the limitations on the time step for time dependent problems indicates that even for steady state problems one should limit the local CFL near shocks to less than one, at least in the transient phase. This is crucial for hypersonic flow.

REFERENCES

1. H. T. Huynh, *Accurate Monotone Cubic Interpolation*, NASA TM 103789, March 1991.
2. A. Jameson, W. Schmidt, and E. Turkel, *Numerical Solutions of the Euler Equations by Finite Volume Methods Usung Runge–Kutta Time-Stepping Schemes*, AIAA Paper 81-1259, 1981.
3. A. Jameson and T. J. Baker, *Multigrid Solution of the Euler Equations for Aircraft Configurations*, AIAA Paper 84-0093, January 1984.
4. A. Lerat and J. Sides, "Efficient Solution of the Steady Euler Equations with a Centered Implicit Method," in *Numerical Methods for Fluid Dynamics, III*, edited by K. W. Morton and M. J. Baines (Clarendon Press, Oxford, 1988), p. 65.
5. H.-C. Lin, *J. Comput. Phys.* **106** (1993).
6. C.-W. Shu and S. Osher, *J. Comput. Phys.* **77**, 439 (1988).
7. C.-W. Shu, *SIAM J. Sci. Statist. Comput.* **9**, 1073 (1988).
8. C.-W. Shu, *Math. Comput.* **49**, 105 (1987).
9. R. C. Swanson, and E. Turkel, *J. Comput. Phys.* **101**, 292 (1992).
10. P. K. Sweby, *SIAM J. Numer. Anal.* **21**, 995 (1984).
11. E. Tadmor, *SIAM J. Numer. Anal.* **25** (5), 1002 (1988).
12. E. Turkel, "Improving the Accuracy of Central Difference Schemes," in *11th International Conference on Numerical Methods in Fluid Dynamics, 1988*, Lecture Notes in Physics, Vol. 323 (Springer-Verlag, New York/Berlin, 1988), p. 568.
13. H. Q. Yang and A. J. Prezekwas, *J. Comput. Phys.* **102** 139 (1992).
14. H. C. Yee, *A Class of High-Resolution Explicit and Implicit Shock-Capturing Methods*, NASA TM-101088, 1989 (unpublished)